

Cite this: *Phys. Chem. Chem. Phys.*,
2022, 24, 26879

Molecular understanding of charge effect on desalination performance in lamellar MoS₂ membranes†

Junhui Yao,^a Chen Chen,^a Jing Zhang,^a Li Zhang,^{ID *a} Wei Zhang,^a Jia-Wei Shen,^{ID *b} and Lijun Liang,^{ID c}

Due to its advantages of superior oxidation resistance, excellent chemical stability and non-toxicity, molybdenum disulfide (MoS₂) has shown prospects in seawater desalination applications. In this manuscript, molecular dynamics (MD) simulation has been employed to explore the effect of charge distribution in MoS₂ nanosheets on the desalination performance of the lamellar MoS₂ membrane. It is found that the model considering the atomic charge better describes the transport behavior of salt solution in the membranes. The water flux passing through the lamellar MoS₂ membrane would be influenced little by the atomic charges in the MoS₂ nanosheet. The lamellar MoS₂ membrane considering the atomic charge distribution shows a screening effect between Na⁺ and Cl⁻ ions.

Received 11th May 2022,
Accepted 23rd September 2022

DOI: 10.1039/d2cp02145e

rsc.li/pccp

1. Introduction

Recently, the shortage of fresh water has become increasingly serious due to rapid population growth and serious environmental pollution. Seawater desalination provides an effective method to obtain fresh water. At present, reverse osmosis (RO) membranes are widely employed in industry owing to their advantages of low energy consumption, simple process and easy operation. However, there are still some disadvantages to reverse osmosis membranes, such as their easy pollution and oxidation and low water permeability. Therefore, it is necessary to design and develop new membrane materials with high water flux and excellent ion rejection rates for seawater desalination.

With the continuous development of nanomaterials, RO or FO (forward osmosis) membranes constructed by assembling nanosheets such as graphene,¹ graphene oxide² (GO), or hexagonal boron nitride³ (h-BN) nanosheets, have been explored by researchers in recent years, while the application of graphene or carbon nanotubes (CNTs) in seawater desalination would present challenges related to human health and environmental concerns.⁴ Recently, molybdenum disulfide (MoS₂) has attracted

extensive attention from researchers. It is a typical two-dimensional transition metal sulfide with a layered structure. It shows not only the structural advantages shared by other two-dimensional materials (such as atomic thickness and high mechanical strength), but also shows excellent chemical stability,⁵ swelling resistance⁶ and low cytotoxicity.⁷

Physical and chemical exfoliation⁸ have been applied to obtain monolayer molybdenum disulfide, and researchers have reported that MoS₂ can be employed to construct semipermeable membranes or improve the desalination performance of commercial RO membranes by adding MoS₂ to them.^{6,9} Membranes prepared from MoS₂ can exist stably in water due to the van der Waals¹⁰ and electrostatic interactions¹¹ between MoS₂ nanosheets. Additionally, compared with GO or MXene, the lack of hydrophilic side groups such as -OH, -COOH or -F makes it difficult for MoS₂ membranes to interact with solvent molecules containing hydroxyl groups,¹² thus preventing its interlayer spacing from increasing. MoS₂ also shows application potential in the field of solar desalination by taking advantage of its strong light absorption ability and high light-heat conversion efficiency.^{13,14}

Large-area MoS₂ sheets have been successfully prepared¹⁵ with the development of metalorganic chemical vapor deposition (MOCVD), which provides the potential for its application in seawater desalination. The MoS₂ membrane could be constructed by utilizing the intrinsic defects¹⁶ in MoS₂ nanosheets, but the pore channels caused by the defects may be too small for water molecules to permeate. If channels of the appropriate diameter could be introduced into a monolayer MoS₂ sheet in a controllable way, effective water permeability could be achieved. Molecular dynamic simulations were first employed

^a Department of Chemistry, Key Laboratory of Surface & Interface Science of Polymer Materials of Zhejiang Province, Zhejiang Sci-Tech University, Hangzhou, 310018, P. R. China. E-mail: lizhang@zstu.edu.cn

^b School of Pharmacy, Hangzhou Normal University, Hangzhou, 310016, P. R. China. E-mail: shen.jiawei@hotmail.com

^c College of Life Information Science and Instrument Engineering, Hangzhou Dianzi University, Hangzhou, 310018, P. R. China

† Electronic supplementary information (ESI) available. See DOI: <https://doi.org/10.1039/d2cp02145e>

to demonstrate the potential of monolayer MoS₂ sheets as desalination membranes. For example, Heiranian *et al.*¹⁷ evaluated the desalination performance of MoS₂ by designing nanoporous MoS₂ nanosheets with different sizes and edges *via* molecular dynamics simulation; only-Mo-edged pores showed a higher flux, and the water flux was 70% higher than that of graphene. Recently, researchers have indicated that MoS₂ membranes with an appropriate pore size could be obtained *via* different methods, such as electron-beam lithography,¹⁸ catalyst-free CVD growth¹⁹ and surface electrochemical reaction.²⁰ For example, Liu *et al.*¹⁸ fabricated nanoporous MoS₂ membranes with 1–10 nm diameters using a highly focused electron beam and transmission electron microscope. Drndić *et al.*²¹ created sub-nanometer vacancies in suspended monolayer MoS₂ *via* Ga⁺ ion irradiation, and the average and maximum diameters of these pores were ~0.5 and ~1 nm, respectively.

In the past few years, the transport mechanisms of water molecules passing through nanoporous MoS₂ membranes have been analyzed from the viewpoints of steric effects, hydrogen bonds and interactions *via* molecular dynamic simulations.^{22,23} Zhou *et al.*²⁴ found that the pore size of MoS₂ nanosheets was sensitive to mechanical strain and could be adjusted by applying tension during the simulation. If the diameter of the nanopore was close to the size of the hydrated ions, various types of ions could be intercepted *via* the monolayer MoS₂ membrane. Cao *et al.*²⁵ reported higher water flux and an ideal ion rejection rate in MoS₂ membranes. This can be attributed to the smaller energy barrier for water molecules passing through the nanopores. Our previous work also indicated that the desalination performance would be influenced by the size of pores²⁶ by analyzing the potential of mean force (PMF) for water molecules and ions and the density distribution profiles of water molecules inside the nanopores.

As discussed in our previous work,²⁷ lamellar membranes fabricated using two-dimensional nanosheets could allow water molecules to pass through the nanosheets with a high speed. Recently, Chu *et al.*²⁸ prepared lamellar MoS₂ membranes *via* cation insertion. The composite membrane could remain intact in aqueous solutions with different pH values, and its permeation performance was not affected by the pH value, which

indicates its potential applications in seawater desalination. Jung *et al.*²⁹ prepared layered MoS₂ membranes using chemical vapor deposition (CVD), and the layered MoS₂ membrane showed high water permeability ($>322 \text{ L m}^{-2} \text{ h}^{-1} \text{ bar}^{-1}$) and ion rejection rate ($>99\%$). Additionally, FO membranes grafted with MoS₂ nanosheets through layer-by-layer assembly were successfully prepared by Sun *et al.*³⁰ The grafting of MoS₂ on the membrane surface gave the FO membrane higher porosity and average pore size, and it showed higher water flux and lower reverse solute diffusion. In addition to the direct preparation of RO membranes with MoS₂, it can also be employed to modify commercial RO membranes. Zhang *et al.*³¹ prepared a nano-composite membrane with high permeability and selectivity by adding MoS₂ nanosheets in a thin-film composite (TFC). Compared to that of the TFC, the hydrophilicity in the composite was enhanced by adding MoS₂ nanosheets in it, which resulted in an increase of water flux. The ion rejection was also improved owing to the screening effect of the membrane matrix as well as the electrostatic attraction/repulsion between the MoS₂ nanosheets and ions. Hirunpinyopas *et al.*³² reported that the permeability of Na⁺/Cl⁻ ions could be reduced owing to the electrostatic repulsion between the MoS₂ surface and ions, and that the water flux passing through it was five times that of graphene oxide membranes. The MoS₂ composite membrane constructed on ceramic hollow fiber by Ma *et al.*³³ showed excellent nanofiltration performance and excellent stability. The interface adhesion between adjacent MoS₂ nanosheets as well as the MoS₂ layer and substrate were enhanced by the formation of a tight and neat separation layer.

Although various MoS₂ membranes have been employed for desalination in experiments, the transport mechanism of water molecules, as well as the separation mechanism of ions passing through the lamellar MoS₂ membrane, is still poorly understood. It is well known that the charge distribution of MoS₂ nanosheets can be modified by changing the functional groups with different electronic effects in the experiment, while the effect of atomic charge distribution on the MoS₂ sheets on their desalination performance and transport mechanism is still unknown. In this work, a lamellar MoS₂ membrane was constructed and the effect of atomic charge distribution on its

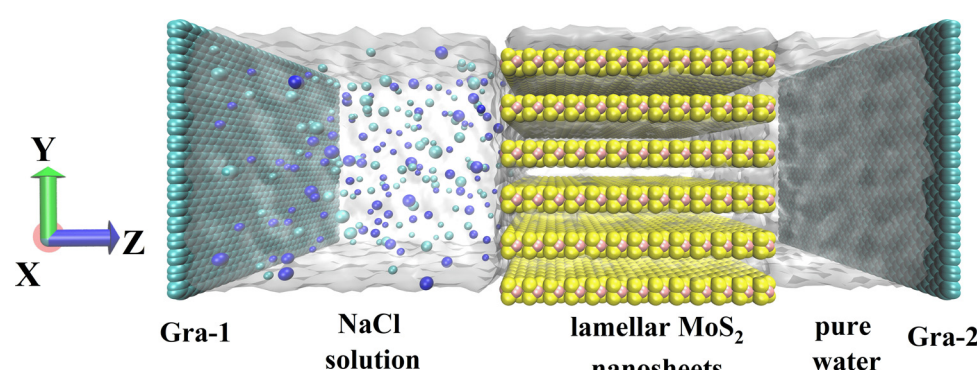


Fig. 1 Model of desalination using the lamellar stacked MoS₂ membrane. Water molecules are shown in a QuickSurf model (white and transparent), and the remaining atoms are shown in a VDW model. Graphene: blue-green, Na⁺: dark blue, Cl⁻: green, Mo: pink, S: yellow.

desalination performance was explored at the molecular level. This will provide theoretical guidance for the synthesis and application of MoS₂ membranes with highly efficient seawater desalination performance.

2. Model construction and simulation details

2.1 Model construction

The model of desalination using the lamellar MoS₂ membrane is shown in Fig. 1; it is similar to the model employed in our previous work.³⁴ First, one MoS₂ nanosheet with a length and width of 7 nm was constructed, and then multiple MoS₂ nanosheets were moved approximately parallel to each other along the y-axis to construct lamellar MoS₂ membranes with different pore widths. Heiranian *et al.*¹⁷ investigated the desalination performance of a monolayer MoS₂ membrane with different pore sizes and pore chemistry using molecular dynamics simulation. However, all the atoms in the MoS₂ nanosheets had a charge of zero during the simulation; that is, the model employed in their work was a model without an atomic charge distribution. Hence, this model is referred to as Heiranian's model. In fact, both the S and Mo atoms in the MoS₂ nanosheets are charged. Therefore, it is necessary to consider the charge distribution on the MoS₂ nanosheets. Herein, the charge of the Mo and S atoms was calculated according to the charge equilibration (Q_{eq}) method,³⁵ and the charges of the Mo and S atoms were 0.734 and -0.367, respectively. These results are consistent with the work of Becker *et al.*³⁶ In order to explore the effect of charge on the separation mechanism of the lamellar MoS₂ membranes, both the atomic charge information and van der Waals (vdW) parameters were considered in the construction of the MoS₂ nanosheets; this model is referred to as the model with charge distribution and compared with the model employed in the works of Heiranian.¹⁷

2.2 Simulation details and force field parameters

The package Gromacs 5.0.7³⁷ was employed to perform the desalination process. As shown in Fig. 1, graphene-1 (blue-green

part in Fig. 1) was moved along the z-direction as a piston when an external force ($f = PA$, where P is the applied pressure and A is the area of the membrane) was applied on it to impel the transport of water molecules³⁸ across the MoS₂ channels and obtain analyzable data. A pressure of 0.1 MPa along the negative-z-direction was applied to graphene-2 as ambient pressure. The pressure³⁹ we chose to apply on graphene-1 was higher than that used in a practical desalination system with the aim of reducing thermal noise and improving the signal-to-noise ratio on the nanosecond time scale during the simulation progress; the rationality and credibility of this approach have been proven in many works.^{40–43} As a seawater desalination membrane, all the atoms in the lamellar MoS₂ membrane were fixed with the aim of preventing out-of-place displacement⁴⁴ and keeping the structural parameters such as pore width constant. The simulation system was divided into two parts: the left side of the MoS₂ membrane was the feed solution (simulated seawater, composed of 0.5 mol L⁻¹ NaCl solution), and the right side of the membrane was the permeating solution (pure water). The size of the simulation box and the number of water molecules and Na⁺/Cl⁻ ions are listed in Tables S1 and S2 (ESI†), respectively. Periodic boundary conditions were implemented in the xy direction to ensure the continuity and integrality of the system.

The transferable intermolecular potential with 3 points (TIP3P) model⁴⁵ was chosen for describing the water molecules, while the LJ parameters for the atoms in the graphene and MoS₂ nanosheets were derived from the CHARMM27 force field.⁴⁶ The force field parameters of the Na⁺ and Cl⁻ ions were derived from the Amber03 force field.⁴⁷ All the interaction parameters used in the simulations are summarized in Table S3 (ESI†). The simulation step was set to 2 fs, and the Nosé–Hoover method⁴⁸ was applied to keep the temperature at around 300 K. In addition, the classic Particle Mesh Ewald method⁴⁹ and Lorentz–Berthelot mixing rule⁵⁰ were used to calculate the long-range electrostatic interaction and LJ interaction between different atoms. The cutoff radius was set to 1.3 nm. The instantaneous configurations in the simulation process were mainly visualized using the software VMD.⁵¹

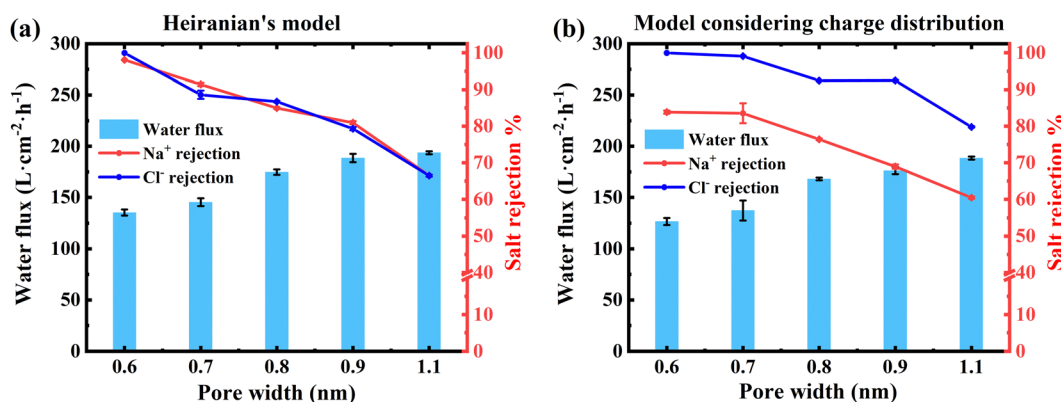


Fig. 2 Water flux and ion rejection rates in MoS₂ membranes described using (a) Heiranian's model and (b) the model considering charge distribution with different pore widths under an external pressure of 100 MPa.

3 Results and discussion

3.1 Effect of molecular model on desalination performance

Heiranian *et al.*¹⁷ explored the desalination performance of nanoporous MoS₂ membranes without atomic charge distribution (called Heiranian's model for short). In the present manuscript, a model with charge distribution is employed to describe the MoS₂ nanosheets. During the process of seawater desalination, graphene-1 is subjected to pressure along the z-direction, which promotes the movement of NaCl solution along the z-direction. Therefore, some water molecules and ions in the feed solution could pass through the lamellar MoS₂ membrane.

According to the work of Liu *et al.*,⁵² the transport behavior of water molecules would be influenced by the interlayer spacing of layer-stacked MoS₂ membranes, and pore width values of ~0.64 nm,⁵³ ~0.98 nm,⁵⁴ ~1.14 nm⁵⁵ have been reported in the relevant works. In order to explore the effect of the molecular model and the influence of pore width on the desalination performance of lamellar MoS₂ membranes, first, MoS₂ membranes with a pore width of 0.6 nm, 0.7 nm, 0.8 nm, 0.9 nm, or 1.1 nm were constructed. The desalination performance of the MoS₂ membranes described using Heiranian's model and the model considering charge distribution with different pore widths under an external pressure of 100 MPa were then calculated, and the results are shown in Fig. 2.

As can be seen from the blue histograms in Fig. 2, the water flux in the lamellar MoS₂ membrane increases with increasing pore width. In order to illustrate this phenomenon more intuitively, the density distributions of the water molecules in one channel of the MoS₂ membranes with different pore widths were calculated and are shown in Fig. S1 (ESI†). For the channel with a pore width of 0.6 nm, only one peak could be detected in the density distribution profile, which indicates that water molecules passed through the channel in the form of a single water molecule chain. With increasing pore width, more peaks could be observed in the water density distribution profiles.

The ion rejection rate is another important index for evaluating desalination performance. Taking Heiranian's model as an example, the rejection rates of Na⁺ and Cl⁻ ions have similar

values and decrease gradually from ~100% to ~65% with the increase of pore width. However, the ion rejection rates in the MoS₂ membrane described by the model considering charge distribution showed different trends. Firstly, the rejection rates of Na⁺ and Cl⁻ ions had different values. Secondly, the rejection rate of Na⁺ ions decreases faster than that of Cl⁻ ions. The density distribution profiles for the Na⁺ and Cl⁻ ions passing through the MoS₂ membrane described by the model considering charge distribution under different pore widths were analyzed and are plotted in Fig. 3. Due to the strong electrostatic repulsion between the negatively-charged S atoms and Cl⁻ ions, most of the Cl⁻ ions are blocked at the port of the membrane (Fig. 3(b)), and the rejection rate of Cl⁻ ions is greater than 90% when the pore width is smaller than 0.9 nm. This also explains the phenomenon of the rejection rate of Cl⁻ ions only decreasing from 100% to 80% with increasing pore width. For Na⁺ ions (hydrated diameter: 6.40 Å⁵⁶), when the pore width is smaller than 0.7 nm, only a small amount of Na⁺ ions could enter and pass through the membrane channel after dehydrating some of the water molecules around them. With increasing pore width, the Na⁺ ions are more likely to enter and pass through the membrane channel owing to the external pressure and the attractive interaction between S atoms and Na⁺ ions, which explains the faster decrease in the Na⁺ ion rejection rate.

Qian *et al.*⁵³ prepared MoS₂ membranes with an interlayer spacing of 0.96 nm using a restacking method, and the larger interlayer spacing (pore width of ~0.66 nm) provided more free spacing and enhanced the interlayer interaction between MoS₂ nanosheets. In order to be consistent with the experiments, as well as to explore the effect of the atomic charge distribution on MoS₂ membranes on seawater desalination, the pore width of lamellar MoS₂ was set to 0.7 nm for further discussion. Different pressures were applied to the graphene sheets to further evaluate the effect of the molecular model on desalination performance. The number of water molecules transferred from the feed solution to pure water in the MoS₂ membranes *versus* simulation time is shown in Fig. S2 (ESI†). The calculation details regarding the water flux and ion rejection rate are listed in the ESI.† As shown in Fig. 4(a), with increasing

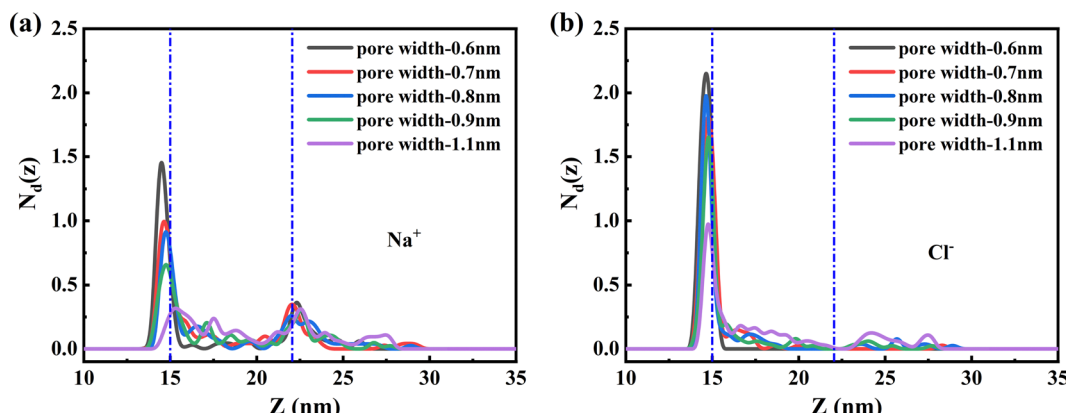


Fig. 3 Density distribution profiles for (a) Na⁺ ions and (b) Cl⁻ ions passing through the MoS₂ membranes described by the model considering charge distribution for different pore widths in the z-direction. Each membrane is between the two blue dashed lines along the z-direction.

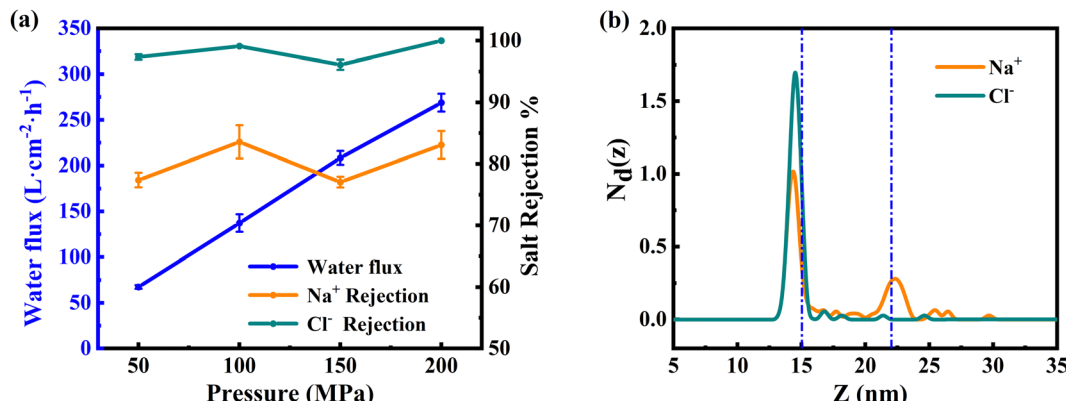


Fig. 4 (a) Desalination performance of the MoS₂ membrane described by the model considering charge distribution under different pressures. (b) Density distribution profiles of ions in the *z*-direction of the MoS₂ membrane described by the model considering charge distribution under 50 MPa. Each membrane is between the two blue dashed lines along the *z*-direction.

pressure, the water flux in the MoS₂ membrane described by the model considering charge distribution increases almost linearly, and the rejection rates of Na⁺ and Cl⁻ remain around 80% and 100%, respectively. During the desalination process, the distance between the graphene-1 sheet and MoS₂ membrane also decreases gradually with increasing simulation time (shown in Fig. S3, ESI†). With the extension of simulation time, most of the water molecules pass through the membrane under the external pressure and reach the permeate side, while the Cl⁻ ions are mainly blocked at the port of the membrane channel.

Different from our previous work,²⁷ the rejection rate values for Na⁺ and Cl⁻ are different, which is also confirmed by the density distribution profiles for the ions in the *z*-direction shown in Fig. 4(b). The height of the density distribution curve for Cl⁻ is higher than that of Na⁺. To perform a straightforward investigation of the transport behavior of the ions, a two-dimensional density map of Na⁺ and Cl⁻ ions near and inside the MoS₂ membrane in the *yz* plane is shown in Fig. 5. As discussed above, due to the strong attractive interaction between S atoms and Na⁺ ions, some Na⁺ ions could enter

the MoS₂ membrane. On the contrary, an obvious difference can be observed in the density map for the Cl⁻ ions (Fig. 5(b)); most of the Cl⁻ ions are blocked in the port of the lamellar MoS₂ membrane (bulk red regions), which explains the 100% rejection rate of Cl⁻ ions.

Moreover, three Na⁺ and three Cl⁻ ions were randomly selected in the MoS₂ membranes considering charge distribution, and their trajectories along the *z*-direction are shown in Fig. 6. As shown in Fig. 6(a), none of the selected Cl⁻ ions could pass through the membrane, and few of the selected Na⁺ ions could enter or pass through the MoS₂ membrane successfully despite the external pressure and attractive interaction with S atoms. When the MoS₂ sheets were described using the model considering charge distribution, the synergistic effect of the attractive interactions and pressure would promote the entry of the Na⁺ ions into the channel of the membrane. However, once the Na⁺ ions enter the channel, their movement may slow due to the attractive interaction between Na⁺ ions and S atoms, as well as that between the Na⁺ ions and Cl⁻ ions blocked in the port of the MoS₂ membrane. On the other hand, the Na⁺ ions prefer to pass through the pore channel under the applied pressure.

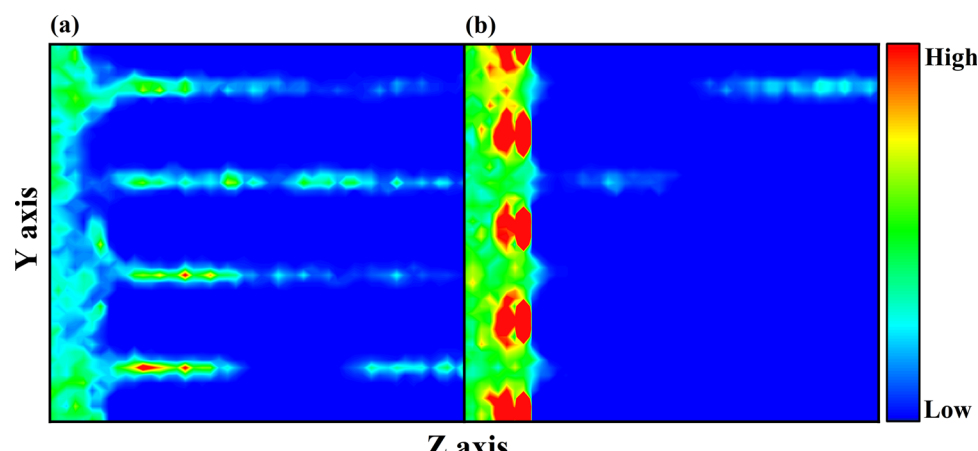


Fig. 5 Density distribution maps of (a) Na⁺ ions and (b) Cl⁻ ions near and inside the MoS₂ membrane described by the model considering charge distribution under 50 MPa.

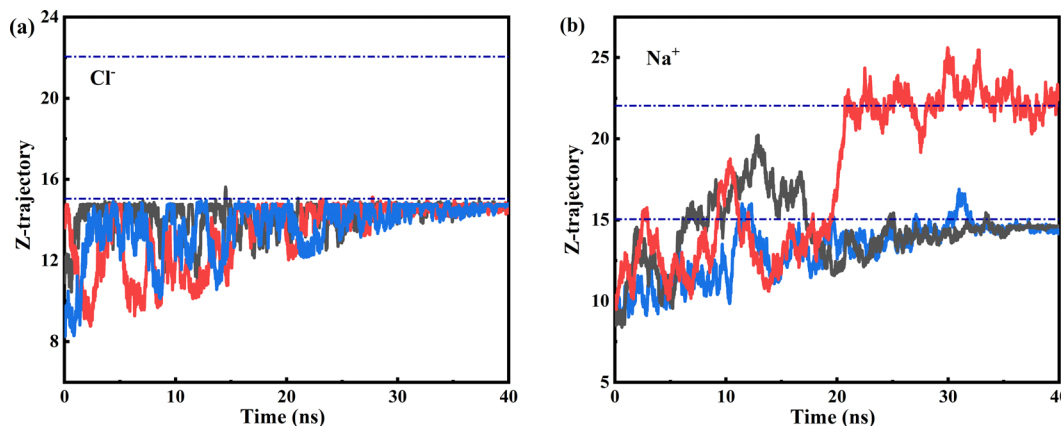


Fig. 6 Trajectories of randomly selected (a) Cl⁻ ions and (b) Na⁺ ions passing through the MoS₂ membrane described by the model considering charge distribution in the z-direction. Each membrane is between the two blue dashed lines along the z-direction.

Therefore, the trajectories of the Na⁺ ions confined in the channel of MoS₂ membranes would show back-and-forth movement.

The water flux and salt rejection values for the lamellar MoS₂ membrane described by Heiranian's model under different pressures were calculated and are shown in Fig. 7(a). The water flux increases linearly with increasing pressure, while the rejection rate of Na⁺ and Cl⁻ changes little; both of them are around 90%. Three ions (Na⁺ and Cl⁻) were randomly selected, and their trajectories along the z-direction are shown in Fig. S4 (ESI†). Neither the selected Na⁺ nor Cl⁻ can pass through the MoS₂ membrane, which suggests that the lamellar MoS₂ membrane shows excellent ion separation. The interception of the Na⁺ and Cl⁻ ions from passing through the membranes is mainly caused by the size-repulsion effect. The diameters of the Cl⁻ and Na⁺ ions with hydration layers are larger than or close to the pore width. For these ions to enter the channel, they must dehydrate and remove some of the water molecules around them. In fact, most of them are blocked in the port of the lamellar MoS₂ membrane, and only a few of them would enter the channel. The density distribution profiles of ions in the z-direction (Fig. 7(b)) and the density map shown in Fig. 8 also support this conclusion.

Based on a comparison of Fig. 4(a) and 7(a), the water flux in the lamellar MoS₂ membrane described by Heiranian's model (Fig. 7(a)) was similar to that described by the model considering charge distribution (Fig. 4(a)). However, obvious differences could be observed between the ion rejection rates of the membranes described by the different molecular models. The lamellar MoS₂ membrane described by the model considering charge distribution shows a screening effect between the Na⁺ and Cl⁻ ions. This indicates that the charge distribution in the MoS₂ nanosheets shows an important effect on their desalination performance.

The density distributions of Na⁺ and Cl⁻ along the z-direction in the MoS₂ membranes described by the different models were calculated and are plotted in Fig. 9. A large quantity of Na⁺ ions was accumulated at the left side of the membrane when the MoS₂ nanosheets were described by Heiranian's model, and only a small amount of Na⁺ can pass through the membrane channel, which reflects a better rejection rate. Additionally, the density distribution profiles for the Na⁺ and Cl⁻ ions are nearly the same. With regards to Cl⁻ ions (Fig. 9(b)), no Cl⁻ ions pass through the pore channel of the MoS₂ membrane. The model considering charge distribution could more closely describe the

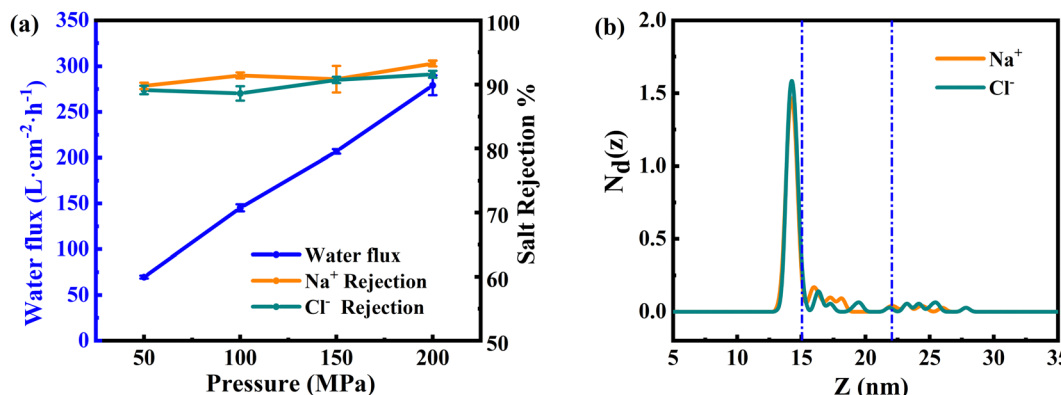


Fig. 7 (a) Desalination performance of the MoS₂ membranes described by Heiranian's model under different pressures. (b) Density distribution profiles of the ions in the z-direction of the MoS₂ membrane described by Heiranian's model under 50 MPa. Each membrane is between the two blue dashed lines along the z-direction.

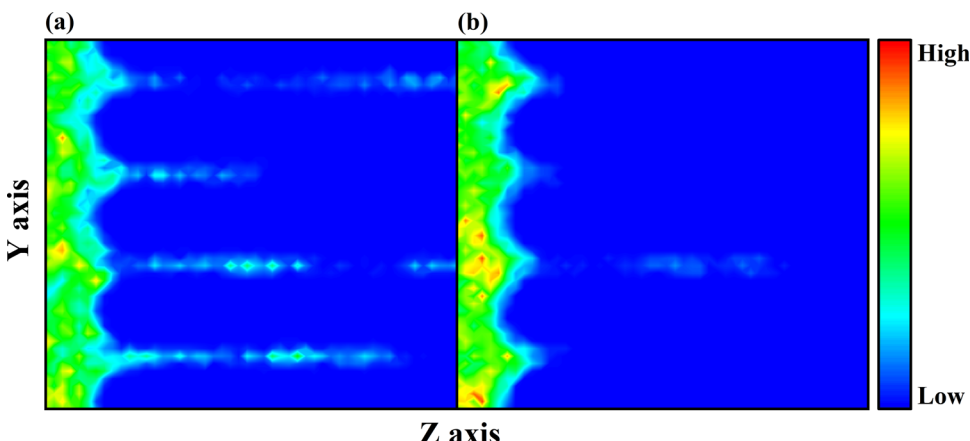


Fig. 8 Density distribution maps of (a) Na^+ ions and (b) Cl^- ions near and inside the MoS_2 membrane described by Heiranian's model under 50 MPa.

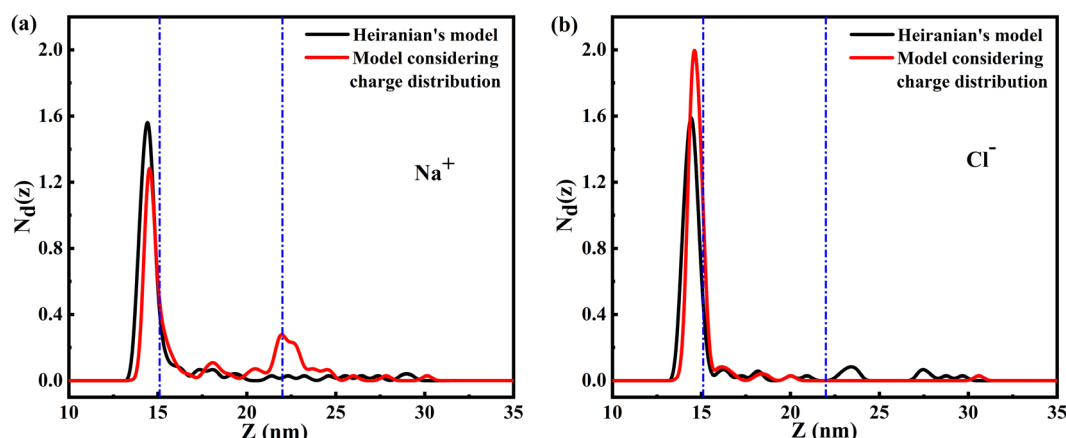


Fig. 9 Density distribution profiles of (a) Na^+ ions and (b) Cl^- ions in the z -direction under 100 MPa for the MoS_2 membrane described by Heiranian's model and the model considering charge distribution. Each membrane is between the two blue dashed lines along the z -direction.

situation in practical application, which will be discussed in the next section.

3.2 Effect of atomic charge on the desalination performance

It has been reported that the charge distribution of MoS_2 nanosheets could be modified by functional groups in experiments;⁵⁷ this could also be realized by adjusting some parameters (e.g. atomic charge distribution) or redesigning the shape of the nanosheets directly in the simulation. For example, Barbosa *et al.*⁵⁸ investigated the role of atomic charges on water mobility by setting different charge information on the Mo and S

atoms. Lu *et al.*⁵⁹ created nanopores with different polar rims by grafting functional groups and adjusting the atomic charge values on the B and N atoms to study water transport through nanopores in BN membranes. Moreover, Beskok *et al.*⁶⁰ reported that the distribution of ions and the transfer velocity of water molecules were obviously changed when the charge distributed around the nanopore was changed from $-3e$ to $+12e$. In order to illustrate the effect of charge on their desalination performance, the atomic charge in the lamellar MoS_2 membranes in our manuscript was adjusted purposefully to construct another two MoS_2 nanosheets with different charge distributions. These MoS_2 nanosheets with adjusted atomic charge were named M-CA-1 and M-CA-2 for short. The atomic charge values for the Mo and S atoms for the different systems are listed in Table 1.

The flux of water molecules passing through the MoS_2 membranes with different atomic charges under 50 and 100 MPa are shown in Fig. 10. It can be observed that the water flux in the membranes described by the model considering charge distribution is slightly lower than that described by Heiranian's model, which may be due to the interaction between the water molecules and MoS_2 sheets. The interaction

Table 1 Atomic charge information for the Mo and S atoms in the different systems

System name	Atomic charge information	
	Mo	S
Hieranian's model	0	0
M-CA-1	0.234	-0.117
M-CA-2	0.534	-0.267
Model considering charge distribution	0.734	-0.367

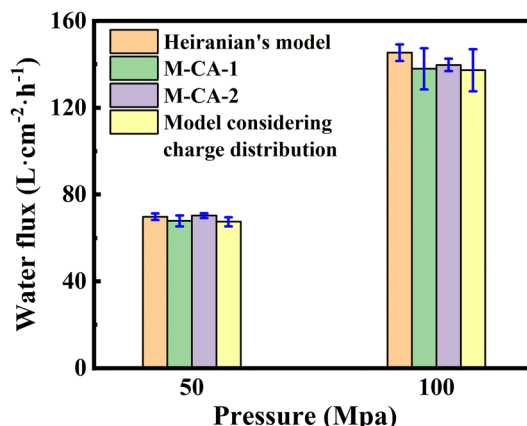


Fig. 10 Water flux passing through the MoS₂ membranes with different atomic charges under 50 MPa and 100 MPa.

energy between water molecules and MoS₂ sheets is enhanced due to the existence of atomic charge (the specific values are listed in Table S4, ESI†), which increases the probability of water molecules being adsorbed around the MoS₂ sheets, which results in the reduction of water flux. In order to better explain this phenomenon, the dipole values for water molecules passing through the MoS₂ membranes along the z-axis under 50 and 100 MPa were calculated and are shown in Fig. 11. The dipole values oscillate between 0 and 1, which indicates that water molecules must adsorb and desorb around the MoS₂ nanosheets constantly, *i.e.*, the conformation of water molecules must be constantly adjusted.

The rejection rates in the MoS₂ membranes with different atomic charges were subsequently calculated and are plotted in Fig. 12. When the atomic charge values for Mo and S atoms in the system are 0, the lamellar MoS₂ membrane (Hieranian's model) does not show the screening effect for Na⁺ and Cl⁻. With increasing atomic charge values for the Mo and S atoms, the rejection rate of Na⁺ gradually decreases from 90% to ~80%, and the rejection rate of Cl⁻ slowly increases and finally approaches 100%. The rejection rates of Na⁺ and Cl⁻ show

opposite trends, and the gap between them becomes larger and larger. The entrance of Na⁺ ions under external pressure becomes easier owing to the attractive electrostatic interaction between the Na⁺ ions and S atoms, while the repulsive electrostatic interaction between the Cl⁻ ions and S atoms results in the increase of the rejection rate for Cl⁻ ions with increasing atomic charge.

The concentration of the feed solution was also reduced to 0.1 mol L⁻¹ in the systems with different charge distributions. As can be seen from Fig. S5 (ESI†), an obvious gap between the rejection rates of Na⁺ ions and Cl⁻ ions still exists, and the rejection rates of Na⁺ and Cl⁻ showed a similar trend compared with the system in which the concentration of the feed solution was 0.5 mol L⁻¹. In other words, the concentration of the feed solution influences the ion rejection rate value, but it does not change the screening effect caused by the atomic charge distributed on the MoS₂ sheets.

In order to explain the transport mechanism of the ions through the MoS₂ membranes with different atomic charges intuitively, the binding free energy between the Na⁺/Cl⁻ ions and MoS₂ nanosheets was calculated with the thermodynamic integration method. The schematic diagram of the thermodynamic cycle is shown in Fig. S6 (ESI†), and the calculation formula is as follows:

$$\Delta G_{\text{bind}} = \Delta G_1 + \Delta G_2 + \Delta G_3 = \Delta G_{\text{ele}} + \Delta G_{\text{vdW}}$$

where ΔG_{ele} represents the free energy when the electrostatic interaction (Coulomb interaction) between ions and water molecules is gradually closed or opened. ΔG_{vdW} represents the free energy when the van der Waals (vdW) interactions between ions and water molecules are gradually closed or opened. ΔG_1 represents the free energy at which the ions are gradually removed from water in the unbound state. ΔG_2 indicates that the free energy approaches zero when the ion is completely removed from the MoS₂ layers. ΔG_3 refers to the free energy when the ion is gradually introduced into the interlayer between MoS₂ in the bound state.

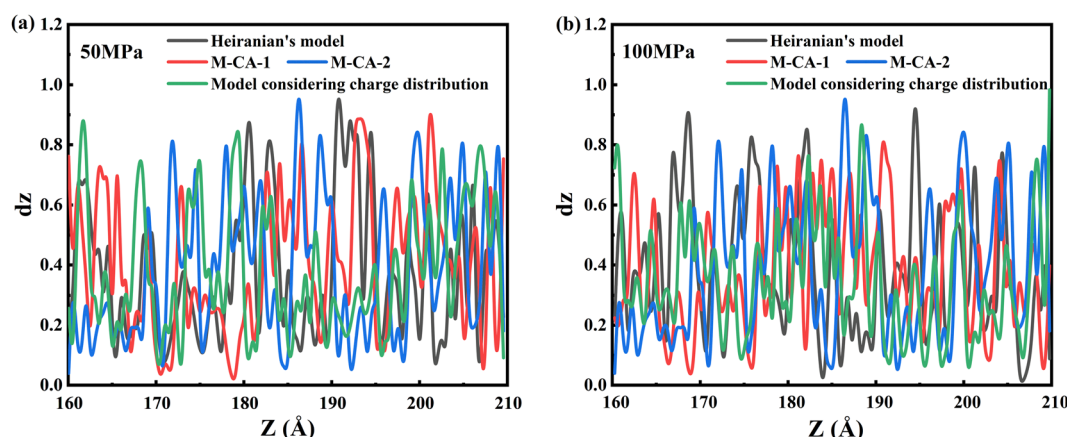


Fig. 11 Values of water dipole as a function of the z-position in the MoS₂ membranes with different atomic charges under pressures of (a) 50 MPa and (b) 100 MPa.

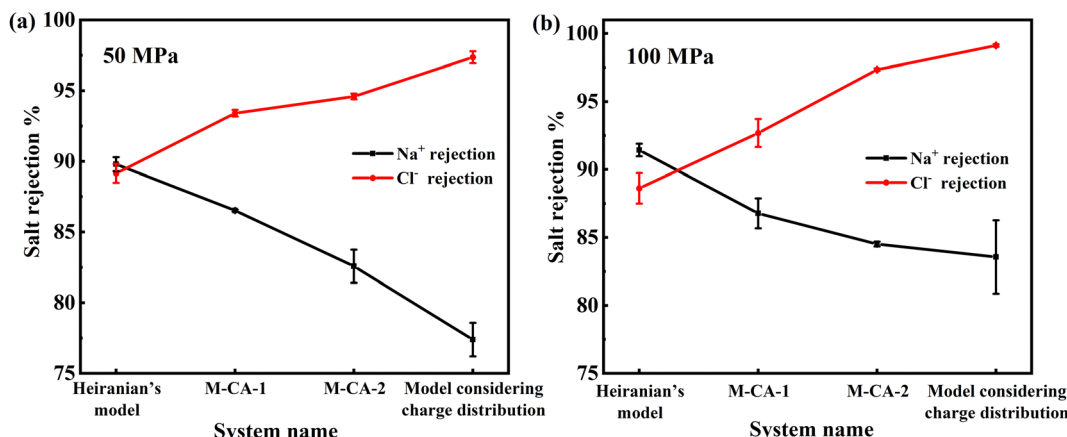


Fig. 12 Trends in the ion rejection rates for Na^+ ions and Cl^- ions in MoS_2 membranes with different atomic charges under (a) 50 MPa and (b) 100 MPa.

As shown in Fig. 13, the binding free energies for Na^+ and Cl^- ions are different, which may be caused by the different hydration behavior of Na^+ and Cl^- ions in the channels of the MoS_2 membranes. Taking Heiranian's model as an example, the pore width of the MoS_2 membrane is about ~ 0.7 nm. The size of the hydrated Na^+ ion is close to the pore width of the MoS_2 membranes, so the hydrated Na^+ ion can enter the channel of the MoS_2 membranes easily, which explains the relatively smaller coulomb interaction between the hydrated Na^+ ion and MoS_2 sheets (shown in Table S5, ESI[†]). Hence, the binding energy for Na^+ is negative, which indicates that the Na^+ ions prefer to exist stably in the channel of the membranes. However, the Cl^- ion (hydration diameter: 7.9 \AA^{35}) must dehydrate some water molecules around it during the process of entering the channel, which suggests that the state of the Cl^- ion confined in the channel of the MoS_2 membrane with a distorted hydration layer was not as stable as that in bulk water; therefore, the coulomb interaction between the Cl^- ion and MoS_2 sheets becomes larger, which results in the positive binding free energy for the Cl^- ion. With increasing atomic charge values on the Mo and S atoms in the MoS_2 sheets, the binding free energy becomes larger, the repulsion between the

S atoms and Cl^- ions becomes increasingly obvious, and the Cl^- ions must overcome a higher energy barrier to pass through the membrane, which explains the better rejection rate for Cl^- ions in the membrane described by the model considering charge distribution. In addition, snapshots of the ions in one channel of the lamellar MoS_2 membrane are shown in Fig. 14. With increasing atomic charge, a greater amount of Cl^- ions are blocked at the port of the membrane due to the electrostatic repulsion. Additionally, the number of Na^+ ions observed in the channel is higher than that for Cl^- ions, and the rejection rate of Cl^- in the model considering the charge distribution is close to 100%, which indicates that an obvious screening effect could be detected in the MoS_2 membranes considering charge distribution.

4 Conclusions

In this work, lamellar MoS_2 membranes were constructed via molecular dynamics simulation to explore the charge effect on their desalination performance. It was found that the water flux passing through the lamellar MoS_2 membrane would be little influenced by the atomic charge. This can be attributed to the disordered state of water molecules in the interlayer of the lamellar MoS_2 membranes, and the transport behavior is mainly affected by pressure.

However, the ion rejection rate would be influenced by the atomic charge owing to the existence of electrostatic interactions. With increasing atomic charge on the Mo and S atoms in the MoS_2 nanosheets, which creates repulsion toward Cl^- ions, it is difficult for the Cl^- ions to enter and pass through the channels of the lamellar membrane, resulting in a $\sim 100\%$ rejection rate. At the same time, the attractive interaction between the S atoms of MoS_2 in the model considering charge distribution and Na^+ ions would cause a lower rejection rate for Na^+ ions. The lamellar MoS_2 membrane considering atomic charge distribution shows a screening effect between Na^+ and Cl^- ions.

Compared with Heiranian's model, the model considering atomic charge distribution can better describe the transfer

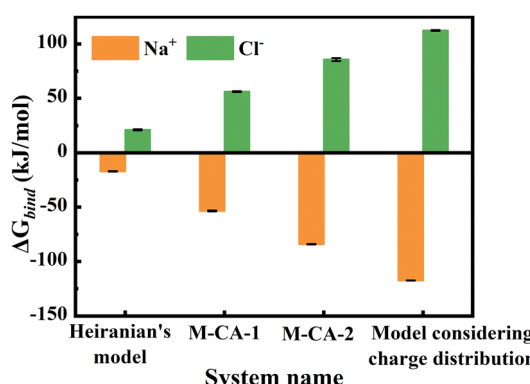


Fig. 13 Binding free energy between Na^+ ions (orange histogram) or Cl^- ions (green histogram) and MoS_2 nanosheets described with different atomic charges.

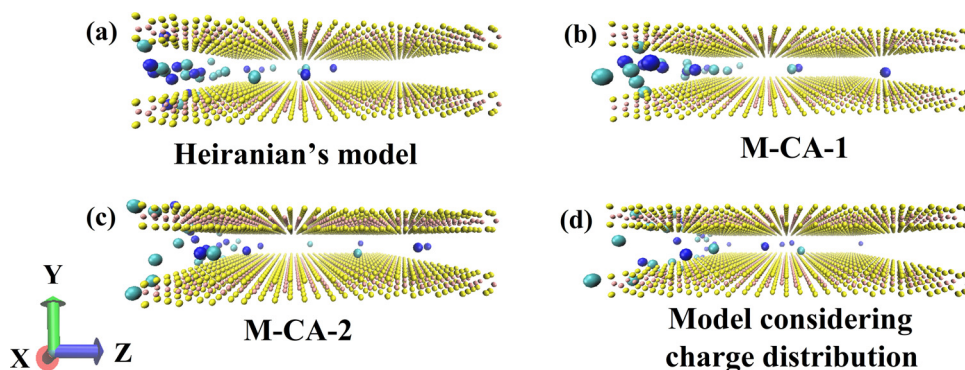


Fig. 14 Snapshots of ions in one of the MoS_2 membrane channels. (a) Heiranian's model, (b) M-CA-1, (c) M-CA-2, and (d) model considering charge distribution. Water molecules are hidden for clearness, Cl^- ions (green) and Na^+ ions (blue) are displayed using the VDW model, and MoS_2 nanosheets are displayed using the CPK model.

behavior of salt solution in nanosheets. This research provides some theoretical guidance and reference for the design of MoS_2 -based membranes with excellent ion-sieving performance in the future.

Author contributions

Junhui Yao: data curation, writing – original draft, investigation. Chen Chen: data curation, investigation. Jing Zhang: data curation, visualization, software. Li Zhang: conceptualization, writing – review & editing. Wei Zhang: supervision. Jia-Wei Shen: formal analysis. Lijun Liang: formal analysis.

Conflicts of interest

There are no conflicts to declare.

Acknowledgements

This work was financially supported by the National Natural Science Foundation of China (Grant No. 21978274 and 21978060).

References

- X. Chen, Y.-B. Zhu, H. Yu, J. Z. Liu, C. D. Easton, Z. Wang, Y. Hu, Z. Xie, H.-A. Wu, X. Zhang, D. Li and H. Wang, *J. Membr. Sci.*, 2021, **621**, 118934.
- L. Zhang, W. Li, M. Zhang and S. Chen, *Nanoscale*, 2020, **12**, 20749–20758.
- C. Chen, S. Qin, D. Liu, J. Wang, G. Yang, Y. Su, L. Zhang, W. Cao, M. Ma, Y. Qian, Y. Liu, J. Z. Liu and W. Lei, *ACS Appl. Mater. Interfaces*, 2019, **11**, 30430–30436.
- S. F. Anis, R. Hashaikeh and N. Hilal, *Desalination*, 2019, **468**, 114077.
- D. Pariari, R. M. Varma, M. N. Nair, P. Zeller, M. Amati, L. Gregoratti, K. K. Nanda and D. D. Sarma, *Appl. Mater. Today*, 2020, **19**, 100544.
- Z. Wang, Q. Tu, S. Zheng, J. J. Urban, S. Li and B. Mi, *Nano Lett.*, 2017, **17**, 7289–7298.
- W. Z. Teo, E. L. Chng, Z. Sofer and M. Pumera, *Chemistry*, 2014, **20**, 9627–9632.
- J. Peng, J. Wu, X. Li, Y. Zhou, Z. Yu, Y. Guo, J. Wu, Y. Lin, Z. Li, X. Wu, C. Wu and Y. Xie, *J. Am. Chem. Soc.*, 2017, **139**, 9019–9025.
- J. Gao, M. Zhang, J. Wang, G. Liu, H. Liu and Y. Jiang, *ACS Omega*, 2019, **4**, 4012–4022.
- K. Tang, W. Qi, Y. Li and T. Wang, *J. Phys. Chem. C*, 2018, **122**, 7027–7032.
- K. S. Lee, Y. J. Park, J. Shim, C.-H. Lee, G.-H. Lim, H. Y. Kim, J. W. Choi, C.-L. Lee, Y. Jin, K. Yu, H.-S. Chung, B. Angadi, S.-I. Na and D. I. Son, *J. Mater. Chem. A*, 2019, **7**, 15356–15363.
- B.-Y. Guo, S.-D. Jiang, M.-J. Tang, K. Li, S. Sun, P.-Y. Chen and S. Zhang, *J. Phys. Chem. Lett.*, 2019, **10**, 4609–4617.
- Q. Wang, Q. Guo, F. Jia, Y. Li and S. Song, *ACS Appl. Mater. Interfaces*, 2020, **12**, 32673–32680.
- Q. Wang, F. Jia, A. Huang, Y. Qin, S. Song, Y. Li and M. A. C. Arroyo, *Desalination*, 2020, **481**, 114359.
- N. A. Simonson, J. R. Nasr, S. Subramanian, B. Jariwala, R. Zhao, S. Das and J. A. Robinson, *FlatChem*, 2018, **11**, 32–37.
- H. Wang, C. Zhang and F. Rana, *Nano Lett.*, 2015, **15**, 8204–8210.
- M. Heiranian, A. B. Farimani and N. R. Aluru, *Nat. Commun.*, 2015, **6**, 8616.
- K. Liu, J. Feng, A. Kis and A. Radenovic, *ACS Nano*, 2014, **8**, 2504–2511.
- P. Waduge, I. Bilgin, J. Larkin, R. Y. Henley, K. Goodfellow, A. C. Graham, D. C. Bell, N. Vamivakas, S. Kar and M. Wanunu, *ACS Nano*, 2015, **9**, 7352–7359.
- J. Feng, K. Liu, M. Graf, M. Lihter, R. D. Bulushev, D. Dumcenco, D. T. Alexander, D. Krasnozhon, T. Vuletic, A. Kis and A. Radenovic, *Nano Lett.*, 2015, **15**, 3431–3438.
- J. P. Thiruraman, K. Fujisawa, G. Danda, P. M. Das, T. Zhang, A. Bolotsky, N. Perea-Lopez, A. Nicolai, P. Senet, M. Terrones and M. Drndic, *Nano Lett.*, 2018, **18**, 1651–1659.
- M. H. Kohler, J. R. Bordin and M. C. Barbosa, *J. Chem. Phys.*, 2018, **148**, 222804.

- 23 A. Fang, K. Kroenlein and A. Smolyanitsky, *J. Phys. Chem. C*, 2019, **123**, 3588–3593.
- 24 W. Li, Y. Yang, J. Weber, G. Zhang and R. Zhou, *ACS Nano*, 2016, **10**, 1829–1835.
- 25 Z. Cao, V. Liu and A. Barati Farimani, *ACS Energy Lett.*, 2020, **5**, 2217–2222.
- 26 J.-W. Shen, J. Li, F. Liu, L. Zhang, L. Liang, H. Wang and J.-Y. Wu, *J. Membr. Sci.*, 2020, **595**, 117611.
- 27 C. Chen, F. Huang, L. Jia, L. Zhang, E. Chen, L. Liang, Z. Kong, X. Wang, W. Zhang and J.-W. Shen, *J. Mol. Liq.*, 2021, **333**, 116024.
- 28 C. Chu, C.-F. Fu, P. Zhang, T. Pan, X. Ai, Y. Wu, P. Cui, Q. Huang and J. Ran, *J. Membr. Sci.*, 2020, **615**, 118520.
- 29 H. Li, T. J. Ko, M. Lee, H. S. Chung, S. S. Han, K. H. Oh, A. Sadmani, H. Kang and Y. Jung, *Nano Lett.*, 2019, **19**, 5194–5204.
- 30 M.-N. Li, X.-F. Sun, L. Wang, S.-Y. Wang, M. Z. Afzal, C. Song and S.-G. Wang, *Desalination*, 2018, **436**, 107–113.
- 31 Y. Li, S. Yang, K. Zhang and B. Van der Bruggen, *Desalination*, 2019, **454**, 48–58.
- 32 W. Hirunpinyopas, E. Prestat, S. D. Worrall, S. J. Haigh, R. A. W. Dryfe and M. A. Bissett, *ACS Nano*, 2017, **11**, 11082–11090.
- 33 H. Zhang, D. Taymazov, M.-P. Li, Z.-H. Huang, W.-L. Liu, X. Zhang, X.-H. Ma and Z.-L. Xu, *J. Membr. Sci.*, 2019, **592**, 117369.
- 34 C. Chen, L. Jia, J. Li, L. Zhang, L. Liang, E. Chen, Z. Kong, X. Wang, W. Zhang and J.-W. Shen, *Desalination*, 2020, **491**, 114560.
- 35 A. K. Rappé and W. A. Goddard, *J. Phys. Chem.*, 1991, **95**, 3358–3363.
- 36 U. Becker, K. M. Rosso, R. Weaver, M. Warren and M. F. Hochella, *Geochim. Cosmochim. Acta*, 2003, **67**, 923–934.
- 37 B. Hess, C. Kutzner, D. van der Spoel and E. Lindahl, *J. Chem. Theory Comput.*, 2008, **4**, 435–447.
- 38 Z. Gu, M. Duan and Y. Tu, *Desalination*, 2022, **523**, 115452.
- 39 L. Zhang, L. Jia, J. Zhang, J. Li, L. Liang, Z. Kong, J.-W. Shen, X. Wang, W. Zhang and H. Wang, *Desalination*, 2019, **464**, 84–93.
- 40 Z. Hu, Y. Chen and J. Jiang, *J. Chem. Phys.*, 2011, **134**, 134705.
- 41 K. M. Gupta, K. Zhang and J. Jiang, *Langmuir*, 2015, **31**, 13230–13237.
- 42 K. Meidani, Z. Cao and A. Barati Farimani, *ACS Appl. Nano Mater.*, 2021, **4**, 6145–6151.
- 43 M. Akhavan, J. Schofield and S. Jalili, *Phys. Chem. Chem. Phys.*, 2018, **20**, 13607–13615.
- 44 J. Zhang, C. Chen, J. Pan, L. Zhang, L. Liang, Z. Kong, X. Wang, W. Zhang and J. W. Shen, *Phys. Chem. Chem. Phys.*, 2020, **22**, 7224–7233.
- 45 J. Liu, G. Shi, P. Guo, J. Yang and H. Fang, *Phys. Rev. Lett.*, 2015, **115**, 164502.
- 46 A. D. MacKerell, D. Bashford, M. Bellott, R. L. Dunbrack, J. D. Evanseck, M. J. Field, S. Fischer, J. Gao, H. Guo, S. Ha, D. Joseph-McCarthy, L. Kuchnir, K. Kuczera, F. T. K. Lau, C. Mattos, S. Michnick, T. Ngo, D. T. Nguyen, B. Prodhom, W. E. Reiher, B. Roux, M. Schlenkrich, J. C. Smith, R. Stote, J. Straub, M. Watanabe, J. Wiórkiewicz-Kuczera, D. Yin and M. Karplus, *J. Phys. Chem. B*, 1998, **102**, 3586–3616.
- 47 Y. Duan, C. Wu, S. Chowdhury, M. C. Lee, G. Xiong, W. Zhang, R. Yang, P. Cieplak, R. Luo, T. Lee, J. Caldwell, J. Wang and P. Kollman, *J. Comput. Chem.*, 2003, **24**, 1999–2012.
- 48 D. J. Evans and B. L. Holian, *J. Chem. Phys.*, 1985, **83**, 4069–4074.
- 49 T. Darden, D. York and L. Pedersen, *J. Chem. Phys.*, 1993, **98**, 10089–10092.
- 50 C. L. Wennberg, T. Murtola, S. Páll, M. J. Abraham, B. Hess and E. Lindahl, *J. Chem. Theory Comput.*, 2015, **11**, 5737–5746.
- 51 W. Humphrey, A. Dalke and K. Schulten, *J. Mol. Graph.*, 1996, **14**, 33–38.
- 52 Y. Liu, Y. Zhao, X. Zhang, X. Huang, W. Liao and Y. Zhao, *Chem. Eng. J.*, 2021, **422**, 130082.
- 53 X. Qian, K. Xie, S. Guo, Q. Liang, S. Zhang, Z. Xiong, H. Zhan, C. Liu, X. Yang, J. Zhu and D. Li, *Chem. Commun.*, 2020, **56**, 7005–7008.
- 54 Z. Wang, Q. Tu, S. Zheng, J. J. Urban, S. Li and B. Mi, *Nano Lett.*, 2017, **17**, 7289–7298.
- 55 X. Lu, U. R. Gabinet, C. L. Ritt, X. Feng, A. Deshmukh, K. Kawabata, M. Kaneda, S. M. Hashmi, C. O. Osuji and M. Elimelech, *Environ. Sci. Technol.*, 2020, **54**, 9640–9651.
- 56 Y. Zhang, T. Fang, Q. Hou, Z. Li and Y. Yan, *Phys. Chem. Chem. Phys.*, 2020, **22**, 16978–16984.
- 57 S. Karunakaran, S. Pandit and M. De, *ACS Omega*, 2018, **3**, 17532–17539.
- 58 J. P. K. Abal and M. C. Barbosa, *Phys. Chem. Chem. Phys.*, 2021, **23**, 12075–12081.
- 59 H. Gao, Q. Shi, P. Král and R. Lu, *J. Phys. Chem. C*, 2019, **123**, 27690–27696.
- 60 C. T. Nguyen and A. Beskok, *Phys. Chem. Chem. Phys.*, 2019, **21**, 9483–9494.